JOURNAL OF MATERIALS SCIENCE 23 (1988) 2666–2675

Electrical properties of α-zirconium phosphate and its alkali salts in a humid atmosphere

Y. SADAOKA, M. MATSUGUCHI, Y. SAKAI, S. MITSUI
Department of Industrial Chemistry, Faculty of Engineering, Ehime University, Matsuyama 790, Japan

Humidity dependence of impedance was examined by using the complex impedance analysis for fine crystalline zirconium bis(monohydrogen phosphate) monohydrate and its alkali salts. The value of C_0 in $C_p(\omega) = C_0(j\omega/\omega_0)^{-\alpha}$ was hardly dependent on the relative humidity and monovalent cation species. The resistive component and its activation energy decreased with increase in the relative humidity and the former was expressed as

$$R = R^* \exp(-E/kT^*) \exp(E/kT)$$

The pre-exponential factor R^*, was hardly influenced by the humidity and decreased when the acidic protons were replaced with monovalent alkali cations. The activation energy of conduction was strongly affected by the degree of orientation and particle size of crystal with layered structure in a whole humidity region and increased by replacing the protons by alkali cations.

1. Introduction

The search for new materials for a humidity sensor has led to the design of inorganic electrolytes. Porous oxide is a material adequate for conventional humidity sensing device [1–3], however, most of the usual ceramic sensors are insulators, so that the impedance is $10^8\,\Omega$cm or more in a low humidity region and it is difficult to detect humidity changes using a conventional impedance meter. In order to overcome this disadvantage, the use of an insoluble inorganic polyelectrolyte or the doping of a mobile alkali cation into porous ceramics have been considered [4–6], while in the latter case it is difficult to control the microstructure and the homogeneity. It seems that the insoluble inorganic polyelectrolyte prepared by the reaction with polybasic acids and certain hydrolysable polyvalent cations is a suitable material for a humidity sensing device. α-zirconium phosphate is known as an insoluble inorganic polyelectrolyte and its impedance is $10^6\,\Omega$cm or below even in a low humidity region. In addition, it is easy to prepare a fine crystal with a well defined particle size [7] and the doping of the small alkali cation is well controlled by the end-point titration method. It has been reported that the electrical conductivity is strongly affected by the moisture in the atmosphere [7–9] and the fine crystalline zirconium phosphate and its alkali salts are superior in humidity sensitivity, response time for a humidity change and reproducibility. Preliminary investigations showed that the impedance–humidity relation for zirconium phosphate was strongly affected by the doping of monovalent cations but it was not obvious that the doping of monovalent cations affected either component of impedance, i.e. carrier concentration or activation energy [9]. In the present paper, the effects on the conductive characteristics observed in a humid atmosphere of crystal size, the orientation of the crystal and the doping of the monovalent cation were examined.

2. Experimental procedure

Some types of zirconium phosphate were prepared using different methods. Firstly amorphous zirconium phosphate was prepared by the precipitation of zirconium phosphate which occurs when an appropriate amount of phosphoric acid is added to zirconyl chloride solution. The white pricipitate obtained was separated from the solution by filtration, washed with distilled and deionized water and dried at 60° C. Two types of α-zirconium phosphate were prepared by refluxing amorphous zirconium phosphate with an excess of phosphoric acid for 100 h (CZP100) and 400 h (CZP400). The other crystal was prepared by the precipitation of zirconium phosphate when adding phosphoric acid to zirconium fluorate solution in a bubbling stream of nitrogen (FZP). Zirconium fluorate solution was prepared by mixing zirconyl chloride solution and hydrofluoric acid solution. The average particle diameter was determined to be 0.55 μm (CZP100), 2.4 μm (CZP400) and 5.8 μm (FZP). The alkali salt was obtained by titrating α-zirconium phosphate suspended in distilled and deionized water with the corresponding alkali hydroxide solution. All of the products were washed with distilled and deionized water and dried at 60° C. Hereafter, the fully and half ion-exchanged sample with monovalent cation, X, referred to as $ZrP(X)_2$ and ZrP(HX), respectively. The powder dried at 60° C was pressed into a disc at $200\,kg\,cm^{-2}$ and the disc with ca. 0.5 mm thickness was then shaped to 10 mm × 10 mm. Next, gold electrodes, 4 mm × 4 mm, were applied to both faces of the disc by the vacuum evaporation method.

0022–2461/88 $03.00 + .12

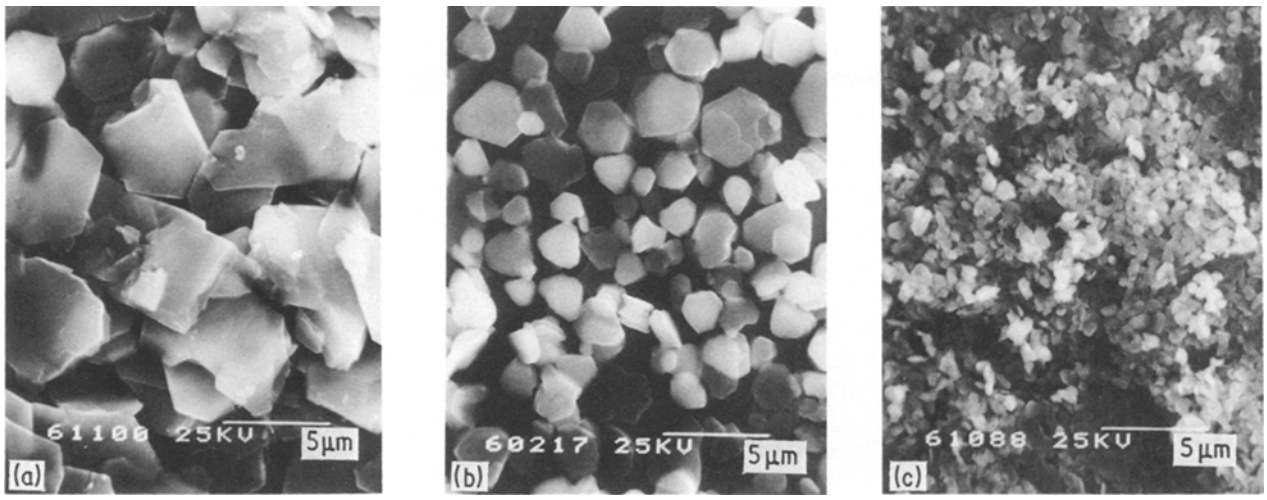

Figure 1 Scanning electron micrographs of compressed powder disc. (a) FZP, (b) CZP400, (c) CZP100.

Humidity–impedance characteristics were measured with impedance meters (10^2–10^6 Hz). Relative humidities (r.h.), ranging from 0 to 90 per cent r.h. were prepared by mixing dry and moist air in controlled proportions in the temperature range of 30 to 45° C. The microstructure was examined by means of scanning electron microscopy. The surface area was determined by the BET method with nitrogen gas as a sorbate. The adsorption isotherm for water was obtained by the gravimetric method. Water content in dry air was examined by thermogravimetry at a heating rate of 5° C min^{-1} in a stream of dried air. Crystalline structure was examined using the standard XRD technique at room temperature.

3. Results and discussion

3.1. Crystal form and microstructure

In Fig. 1 photographs of the surface of the compressed powder are shown. For CZP and FZP, it was confirmed that the sample required a good layered crystalline structure and the *ab* plane of most of the crystal was oriented perpendicular to the direction of the compression and the degree of orientation increased with increasing particle size. The ratio of the length of the *ab* plane and the *c* axis increased with an increase in particle size.

In addition the surface and the fractured face of the disc for ion-exchanged CZP100 are shown in Figs 2 to 4. It is clear that the particle size and form were hardly influenced by the monovalent cation species. This observation convinced us of the results of surface area measurements described in the next section. On the other hand, the crystal has a layered structure and the interlayer distance was influenced by the monovalent cation species and/or the degree of the ion exchange as well-known [10]. The interlayer distances determined by the XRD technique are summarized in Table I. The interlayer distance confirmed in this work was in fair agreement with the value reported by other workers [10, 11]. For CZP400 and FZP, the interlayer distance determined to 0.758 nm and 0.757 nm, respectively, was hardly influenced by the crystal size.

TABLE I R^* values in Equation 6 and interlayer distance

Sample	R^* (Ω cm)	Interlayer distance (nm)		
		(this work)	[11]	[10]
$ZrPH_2$	1000	0.756	0.756	0.756
$ZrPLi_2$	25	0.880	0.850	0.880
$ZrPNa_2$	3.45	0.845	0.851	0.842
$ZrPK_2$	7.69	0.895	0.890	0.890
ZrPHNa	0.40	0.786	0.765	0.765

3.2. Water contents and water adsorption isotherms

Water loss curves for all samples are shown in Fig. 5. The TGA curve for $ZrPH_2$ indicates that the sample lost weight rapidly up to ca. 200° C and then the weight becomes constant at 400° C. Further heating to 700° C gave rise to the weight loss. These observed weight losses correspond to the release of water. For CZP100, the water of crystallization was released by heating up to 200° C and this temperature had to be raised as the crystal size increased, while the amount of water of crystallization and the dehydration temperature of the $Zr(HPO_4)_2 \rightarrow ZrP_2O_7$ was hardly affected by the crystal size. For $ZrPH_2$ and ZrPHNa, the two plateaus were observed in a TGA curve, while only one plateau was observed for $ZrPNa_2$ and $ZrPK_2$. These characteristics closely resemble the results reported by Dyer *et al.* [11] and indicate the following compositions: $Zr(HPO_4)_2 \cdot H_2O$, $Zr(LiPO_4)_2 \cdot 1.3H_2O$, $Zr(NaPO_4)_2 \cdot 1.1H_2O$, $Zr(KPO_4)_2 \cdot H_2O$ and $Zr(HPO_4)(NaPO_4) \cdot 0.75\,H_2O$.

Fig. 6 shows the humidity dependence of the coverage of adsorbed water for CZP and FZP. The coverage of water was determined from the water adsorption isotherm and the surface area determined by the BET method with nitrogen adsorbate. The surface area, S_{N2}($m^2\,g^{-1}$), was 7.3, 5.6 and 1.9 for CZP100, CZP400 and FZP, respectively. The increase in the coverage with particle size suggests that the surface which is parallel to the *ab* plane in the crystal has a more hydrophilic nature than the vertical plane. This difference may be realized qualitatively by the crystal structure and configuration of elements.

In Fig. 7, the relation between coverage of water and relative humidity for alkali salts of CZP100 is shown. The coverage of water is affected by the

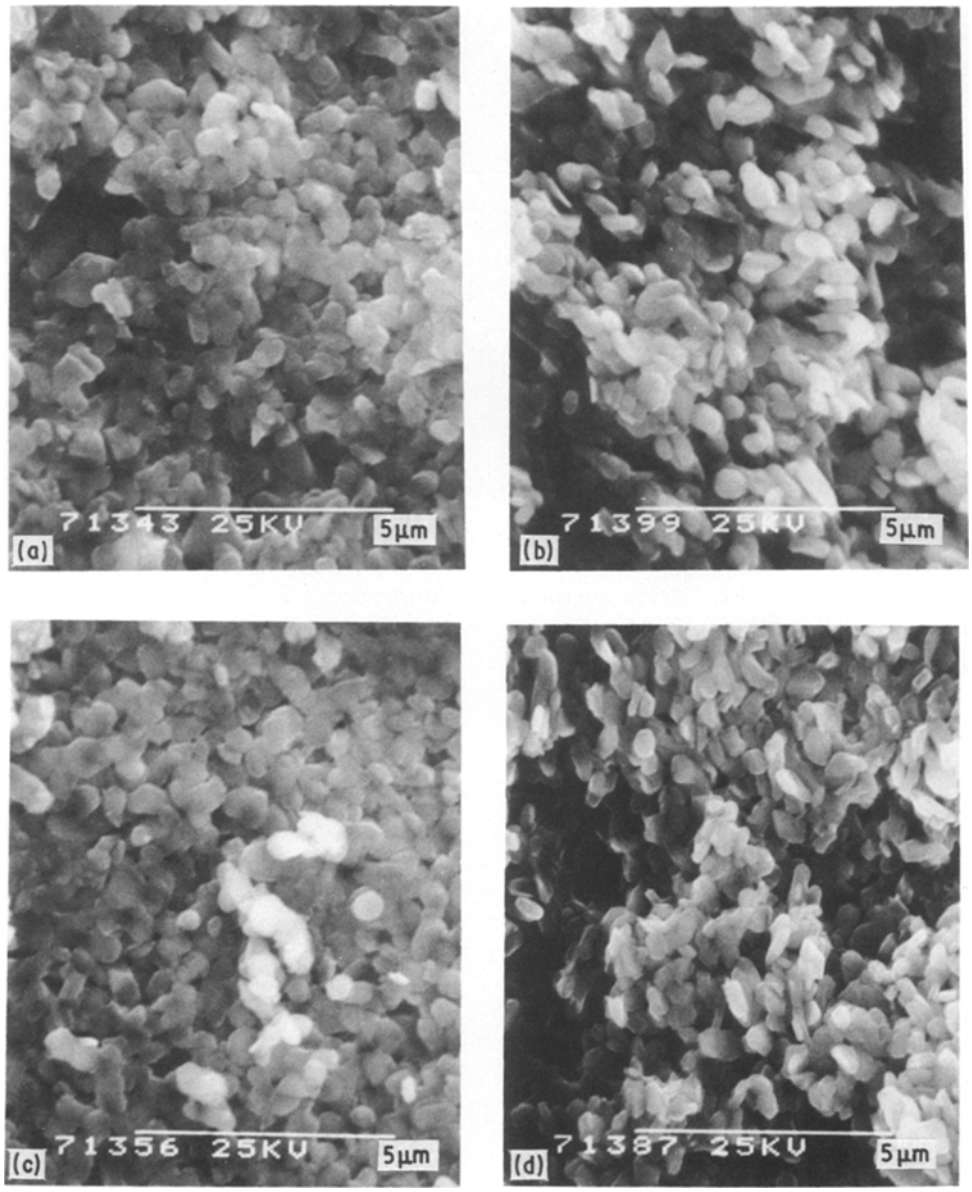

Figure 2 Scanning electron micrographs of compressed powder disc of CZP100 and its alkali salts: (a) surface $ZrPH_2$, (b) fractured face $ZrPH_2$, (c) surface ZrPHNa, (d) fractured face ZrPHNa.

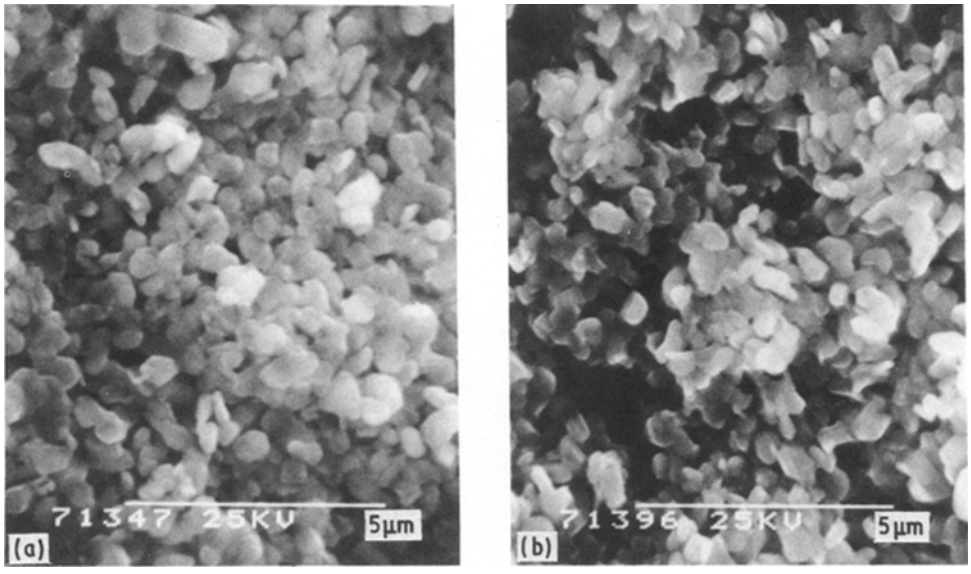

Figure 3 Scanning electron micrographs of compressed powder disc of CZP100 and its alkali salts: (a) surface $ZrPLi_2$, (b) fractured face $ZrPLi_2$, (c) surface $ZrPNa_2$, (d) fractured face $ZrPNa_2$.

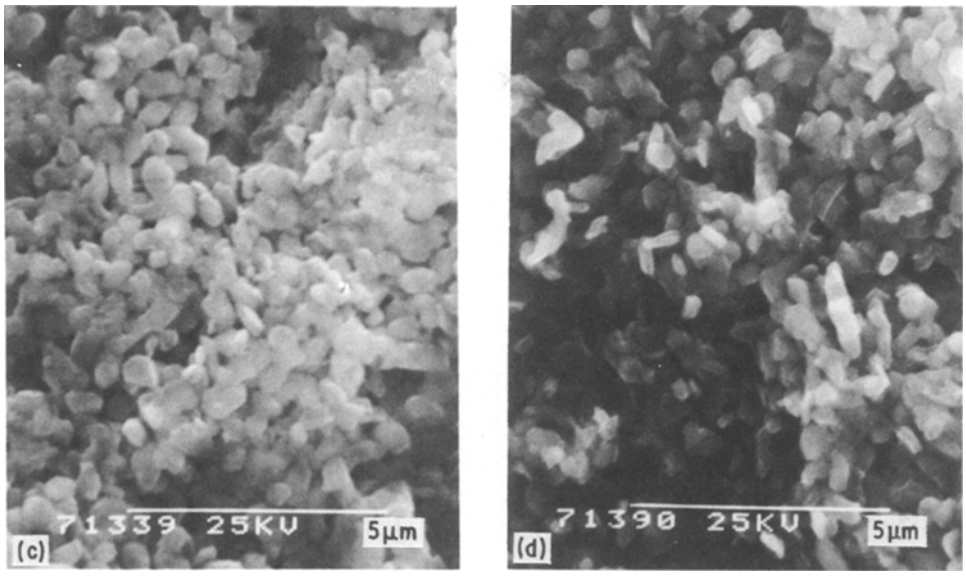

Figure 3 Continued.

monovalent species and is increased by replacing the proton by monovalent alkali cations. The surface area determined by the BET method was 7.3 $m^2 g^{-1}$, 10.0 $m^2 g^{-1}$, 11.0 $m^2 g^{-1}$, 7.7 $m^2 g^{-1}$ and 7.9 $m^2 g^{-1}$ for $ZrPH_2$, $ZrPLi_2$, $ZrPNa_2$, $ZrPK_2$ and ZrPHNa, respectively and is hardly influenced by the monovalent cation species. For FZP and its alkali salts, the coverage of water is increased by replacing the acidic protons with alkali cations, but the ordering of the degree of the coverage is not consistent with that for the alkali salts of CZP and the increase in the surface area was confirmed by replacing the acidic protons with lithium, sodium and potassium. This variation of the surface area for FZP is not suitable for using as a sensing device since it is difficult to control the particle size.

3.3. Equivalent circuit

The impedance of a sample was measured over the temperature range of 30–45° C, at frequencies between 10^2 and 10^6 Hz. Some complex impedance plots are shown in Fig. 8. Similar results were also obtained for the other samples. For all the samples, a single semicircle, whose centre lies under the real axis was found all of which passed through the origin. In addition, a second tail was observed in the high humidity region. This tail may arise from the interfacial polarization. Casciola and Fabiani [12] reported that the semicircle region was dominated by the polycrystalline sample impedance, whereas a second tail represented the contribution of the sample-electrode interface. These observed results may be represented with an appropriate equivalent circuit as shown in Fig. 8, in which the component corresponds to the interfacial polarization is omitted for clarity. The depressed semicircle which appeared in the high frequency region in the complex impedance plot can be adequately expressed by Equation 1

$$Z(\omega) = Z_0/[1 + (j\omega/\omega_0)^{(1-\alpha)}] \quad (1)$$

where $Z(\omega)$ is the complex impedance at an angular frequency ω, Z_0 the low frequency, real-axis intercept, ω_0 the relaxation angular frequency at the maximum height of the semicricle, α the depression parameter

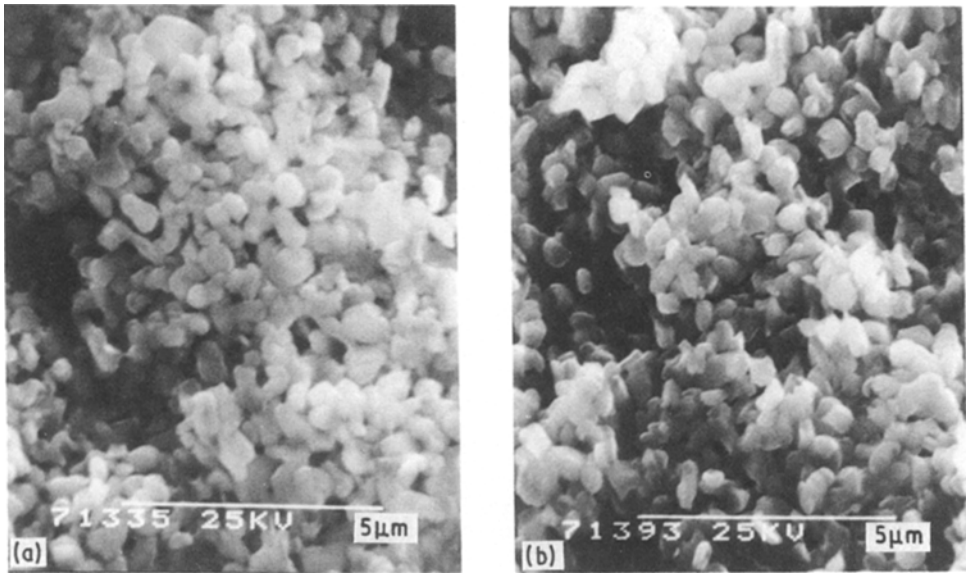

Figure 4 Scanning electron micrographs of compressed powder disc of CZP100 and its alkali salts. (a) surface $ZrPK_2$ (b) fractured face $ZrPK_2$.

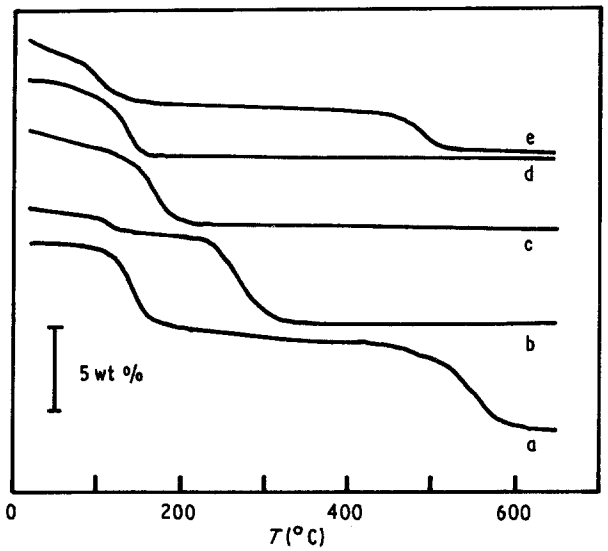

Figure 5 TG curves for samples. a, $ZrPH_2$; b, $ZrPLi_2$; c, $ZrPNa_2$; d, $ZrPK_2$; e, ZrPHNa. Heating rate 5° C min^{-1}, flow rate of dry air 40 ml min^{-1}. Weight increases upwards on the vertical scale.

($\theta = \pi\alpha/2$) and $j = \sqrt{-1}$, respectively. The equivalent circuit corresponding to the impedance spectrum of Fig. 8 consists of a frequency dependent capacitor $C_p(\omega)$ and a frequency independent resistor R_p. These parameters are described by the following equations

$$Z_0 = R_p \quad (2)$$

$$C_p(\omega) = C_0 (j\ \omega/\omega_0)^{-\alpha} \quad (3)$$

$$R_p C_0 \omega_0 = 1 \quad (4)$$

The limiting case of $\theta = 0$ represents an equivalent circuit consisting of lumped RC components with a zero depression angle. The value of θ for $ZrPH_2$ is small and hardly dependent on the relative humidity and the particle size. For alkali salts the value of θ is considerably larger than that of $ZrPH_2$ and increases with an increase in relative humidity as summarized in Table II. It seems that the increase in the θ value which occurs when the acidic protons are replaced with an alkali cation is caused by the diversification of conduction path and/or mechanism but further detailed consideration is difficult. While the capacitive component C_0 obtained by using the Equations 3 and 4 is poorly dependent on the monovalent species and humidity as shown in Table III, the resistive component R_p decreases with an increase in the humidity for all samples and a decrease in the particle size for the proton form.

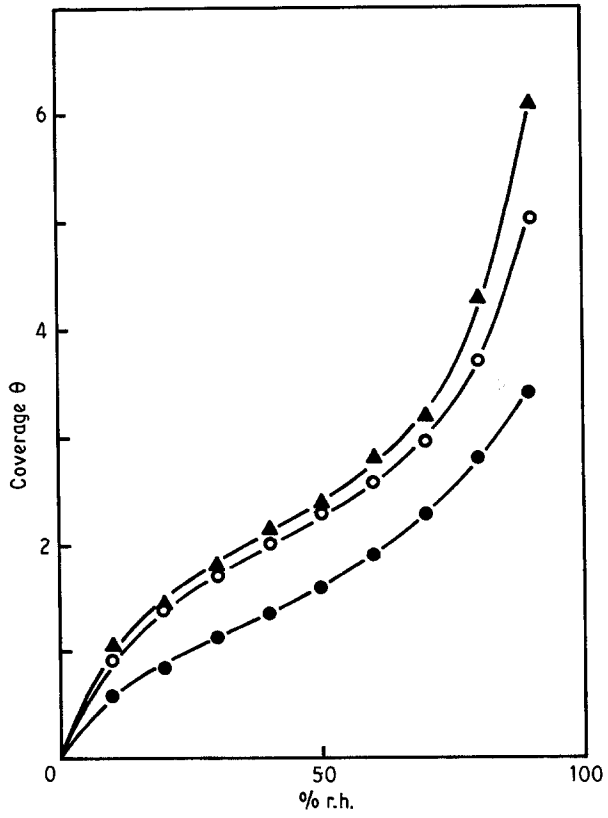

Figure 6 Water adsorption isotherms at 30° C. ● CZP100, ○ CZP400, ▲ FZP.

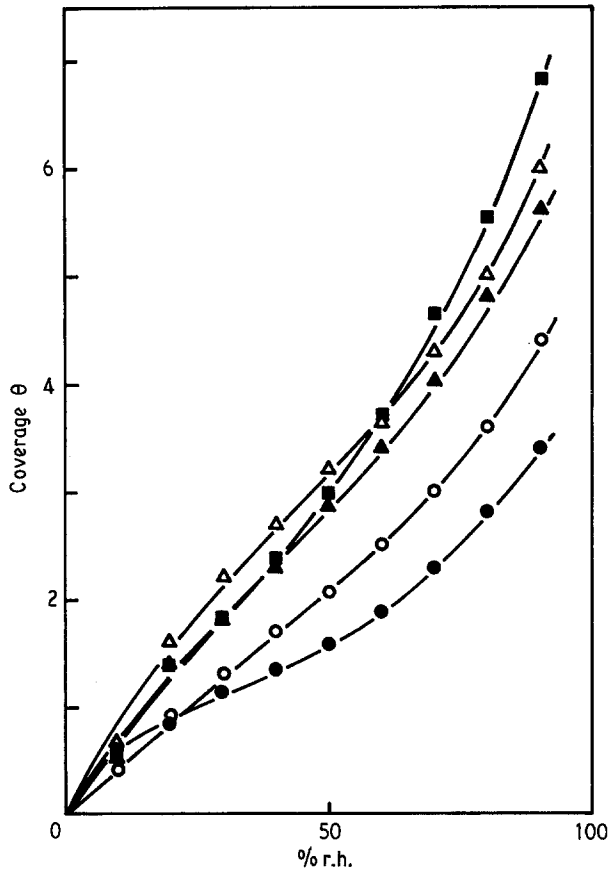

Figure 7 Water adsorption isotherms at 30° C. ● $ZrPH_2$, ○ $ZrPLi_2$, ▲ $ZrPNa_2$, △ $ZrPK_2$, ■ ZrPHNa.

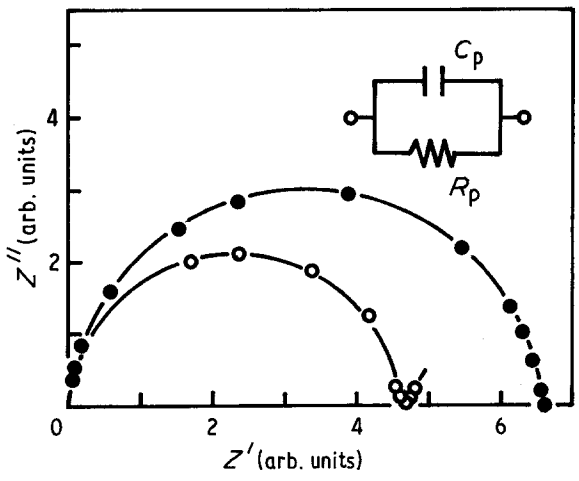

Figure 8 Complex impedance plots and equivalent circuit for CZP100. ● 20% r.h., ○ 60% r.h.

TABLE II θ value in complex impedance plot

Sample	θ (deg) at humidity of					
	10% r.h.	20% r.h.	40% r.h.	60% r.h.	80% r.h.	90% r.h.
$ZrPH_2$	6	6	6	6	7	8
$ZrPLi_2$	10	9	8	8	9	16
$ZrPNa_2$	10	10	10	11	13	19
$ZrPK_2$	12	12	14	16	21	22
ZrPHNa	13	13	13	13	13	16

3.4. Conduction model

In general, the resistivity dependence on temperature is expressed as

$$R = R_0 \exp(E/kT) \quad (5)$$

where R_0 is the pre-exponential factor, E the activation energy for conduction, k the Boltzmann constant and T the absolute temperature. However, for a series of the results, the good linear relation between log R at a certain temperature and E was confirmed and the slope of this line was considerably smaller than $1/kT$ value. This relation can be expressed as Equation 6 instead of Equation 5

$$R = R^* \exp(-E/kT^*) \exp(E/kT) \quad (6)$$

where R^* is the pre-exponential factor and T^* a constant. Equation 6 is well known as the Meyer–Neldel (MN) rule [13]. Meyer and Neldel found that for some oxide semiconductors when the semiconductor is prepared or annealed under different conditions, the activation energy varies and the pre-exponential factor in Equation 5 depends exponentially on the activation energy. This rule is an empirical relation which has been observed in very many different materials such as many types of semiconductor and ionically conducting crystals and glasses [14–17]. For ionic conductors, it has been reported that the MN rule is an approximate relation valid for ionic crystals with either Frenkel, Schottky or interstitial disorder [18]. While some explanations of this relation were proposed, recently, Dyre [17] proposed the phenomenological model based on the hopping of the localized charge carrier and the exponential probability distribution of the energy barrier. According to this model, the d.c. conductivity is expressed as

$$\sigma = CS\gamma_0 (T - TS) \exp(E/kT^*) \times \exp(-E/kT) \quad (7)$$

where γ_0 is the attempt frequency of charge, C is a constant depending on the concentration of localized charge carrier and S is equal to $(1 - T/T^*)$. By adopting the Scher–Lax approach [19], the jump frequency is given by $\gamma = \gamma_0 \exp(-E/kT)$ where E is the activation energy barrier. The maximum jump frequency is γ_0 (corresponding to $E_{min} = 0$) while the minimum jump frequnecy is given by $\gamma_{min} = \gamma_0 \exp(-E_{max}/kT)$ where E_{max} is the maximum energy barrier. In this case, the normalized jump frequency distribution is given by

$$P(\gamma) = (1 - S)(\gamma/\gamma_0)^{-S}/\gamma_0$$

In addition, this relation can be realized by another model. Ion hopping rates, ω_p, are thermally activated and can be expressed as

$$\omega_p = \omega_0 \exp(S/k) \exp(-H/kT) \quad (8)$$

and the magnitude of ionic conductivity is effectively determined by the product of ion hopping rate and a carrier concentration term [20]

$$\sigma = Ne^2a^2c(1 - c)\,\delta k^{-1} T^{-1}\omega_0 \times \exp(S/k) \exp(-H/kT) \quad (9)$$

where N is the number of lattice sites available for the mobile ions, e is the electric charge, a is the jump distance, c is the fractional occupancy of the mobile ion sites, δ is a correlation factor, ω_0 is the fundamental vibrational frequency of the mobile ions, S and H are the conduction entropy and enthalpy, respectively. In this model, by assuming that the entropy is equal to H/T^*, Equation 6 can be introduced.

The MN rule is a result of the very common relationship betwen enthalpies and entropies for the activated process and the σ^* term is not influenced by the activation process. While there still remains considerable theoretical uncertainty about the origin of this relationship, it is preferable to examine the effects of some factors on the electrical conduction behaviour since the pre-exponential factor unaffected by the activation process can be estimated by using the MN rule.

3.5. Humidity dependence of resistive component

3.5.1. Proton forms

The resistivity for all samples decreased quasi-exponentially with an increase in the humidity. It can

TABLE III C_0 value in complex impedance plot

Sample	C_0 (pF cm^{-1}) at humidity of					
	10% r.h.	20% r.h.	40% r.h.	60% r.h.	80% r.h.	90% r.h.
$ZrPH_2$	1.82	1.74	1.69	1.74	–	–
$ZrPLi_2$	2.18	2.20	2.17	2.03	–	–
$ZrPNa_2$	2.55	2.51	2.31	2.37	–	–
$ZrPK_2$	2.73	2.51	2.02	–	–	–
ZrPHNa	2.90	2.87	2.45	–	–	–

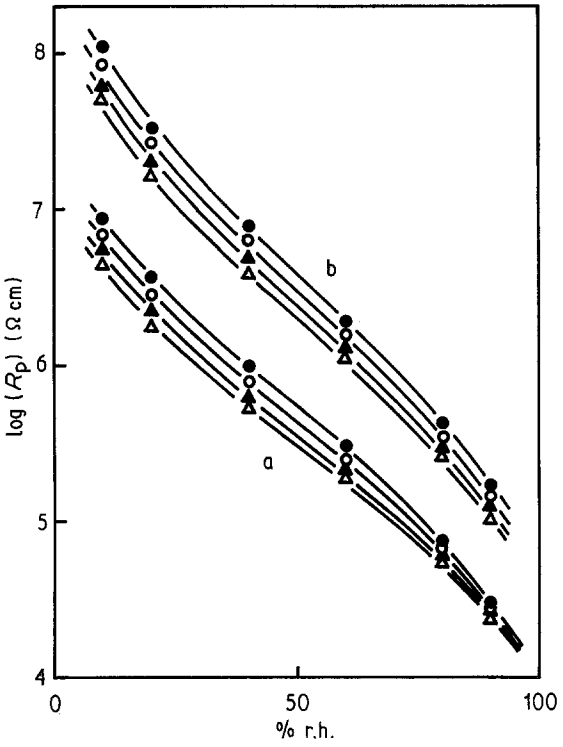

Figure 9 R_p dependence on humidity for (a) CZP400 and (b), FZP. ● 30° C, ○ 35° C, ▲ 40° C, △ 45° C.

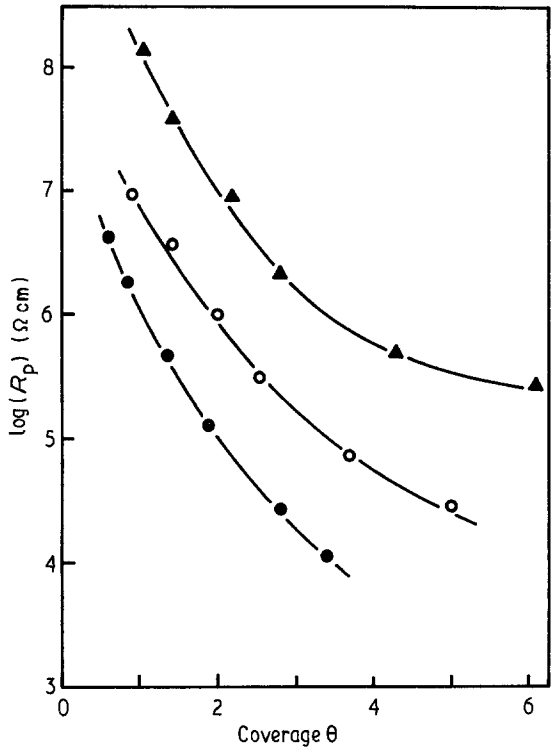

Figure 10 R_p dependence on the coverage of physisorbed water. ● CZP100, ○ CZP400, ▲ FZP.

be assumed that this dependency is caused by the variations of the number of water of crystallization or of the physisorbed water. Since the equilibrium value of the resistivity was achieved within about 5 min after setting a humidity except at 90 per cent r.h. and the reproducibility for a humidity change was observed, the latter case was considered as the origin of this dependency. In Fig. 9, the relation between log R_p and relative humidity for CZP400 and FZP is shown. The resistivity at each humidity increased with an increase in the particle size and its dependence on surface area is considerably higher than that interpreted from the relationship ($R_p^{-1} \propto$ surface area) confirmed in the porous ceramics reported in previous papers [21, 22]. To remove the influence of the coverage of water, the resistivity dependence on the coverage of water was shown in Fig. 10. At a certain coverage, the resistivity dependence on surface area could not be recognized by the relationship. As an origin of this discrepancy, the difference of the surface state which seriously affects the conduction parameters may be considered. For this material it was accepted that conduction occurs on the particle surface and the acidic proton and/or dissociated physisorbed water acts as a main carrier.

As shown in Fig. 6, the mean coverage of the physisorbed water increased with an increase in the particle size and this dependency could be realized by the differences of the ratio of the surface area of the faces defined in parallel and vertical to the *ab* plane for the crystal and of the hydrophilicity of each defined face. It seems that the concentration of the acidic protons on the surface defined in parallel to the *ab* plane is considerably higher than that of the surface formed vertical to the *ab* plane. This difference may affect the conduction parameters. For all samples an electrical field was applied in the vertical direction to the observed faces shown in Fig. 1. For CZP400 and FZP, the *ab* plane was clearly oriented perpendicular to the electric field. The activation energy decreased monotonically with an increase in the coverage and increased with an increase in the particle size (Fig. 11). The particle size dependence of the activation energy can be interpreted in terms of the activation energy of the conduction in the *ab* plane being lower than that in the *c* axis direction. If the proton is a main carrier and the concentration of mobile protons which exist on the surface increases with increasing humidity, the R_0 in Equation 5 may decrease. However, as shown in Fig. 12, the logarithm of R_0 increased with a decrease in the activation energy and the activation energy decreased with humidity. The good linear relation

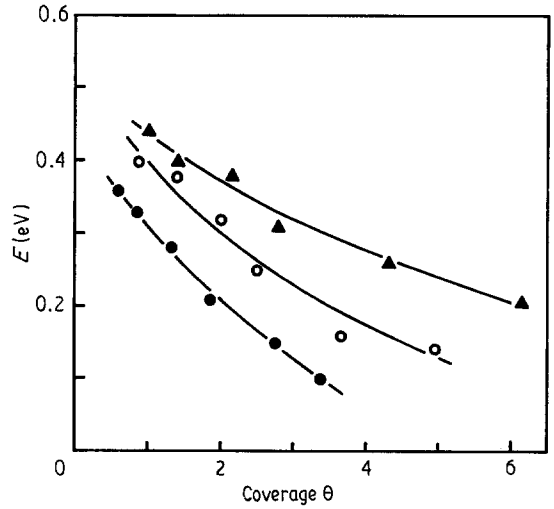

Figure 11 Activation energy dependence on the coverage of physisorbed water. ● CZP100, ○ CZP400, ▲ FZP.

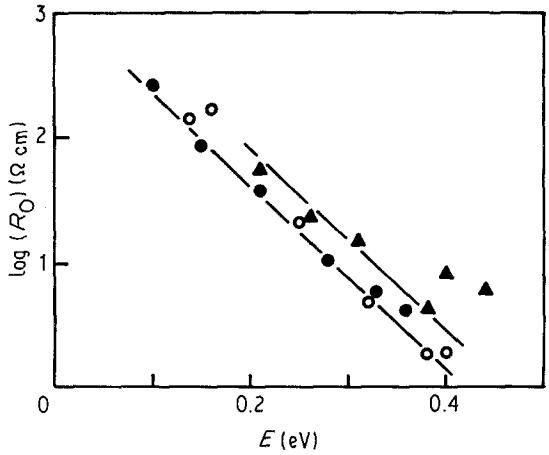

Figure 12 Relation between R_0 and E. ● CZP100, ○ CZP400, ▲ FZP.

between log R_p and E was confirmed and the slopes of these lines were considerably smaller than $1/kT$ value (Fig. 13). These confirmed relations can be expressed as Equation 6 instead of Equation 5. The value of the R^* estimated by using Equation 6 increase slightly with an increase in the particle size. From these observed results, it was confirmed that the decrease in the resistivity by water adsorption was due to the decrease in the activation energy and the R^* was hardly influenced by the coverage of water.

Alberti *et al.* [23] reported that the activation energy for conduction in anhydrous zirconium hydrogen phosphate was ca. 0.8 eV for temperatures below 220° C. Anderson *et al.* [24] found that the activation energy in zirconium phosphate monohydrate was ca. 0.25 eV and independent of the particle size while no observations regarding the orientation degree of the particle were done. The distinction between the observed activation energy in the lower humidity region in this work and the values reported by other workers may be caused by the differences between the hydration degree and/or the orientation degree.

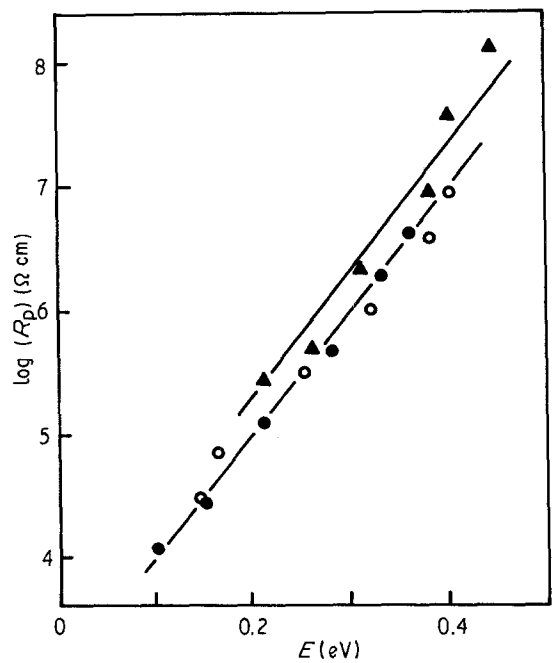

Figure 13 Relation between R_p and E. ● CZP100, ○ CZP400, ▲ FZP.

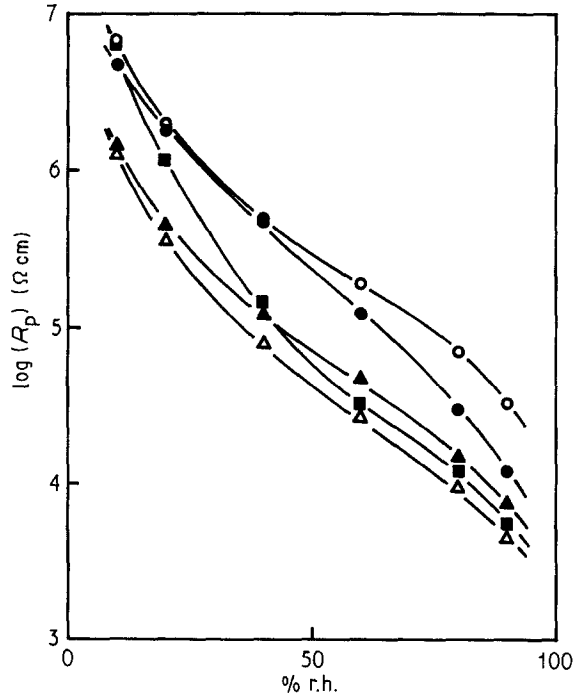

Figure 14 Humidity dependence of R_p at 30° C. ● $ZrPH_2$, ○ $ZrPLi_2$, ▲ $ZrPNa_2$, △ $ZrPK_2$, ■ ZrPHNa.

3.5.2. Alkali forms

In Fig. 14 the humidity dependence of the resistive component at 30° C was shown for CZP100 and its salts. While the resistivity of $ZrPLi_2$ was higher than that of $ZrPH_2$ especially in a high humidity region, the resistivity was lowered in a whole humidity region by replacing the acidic protons with sodium or potassium. It was expected that this variation of the resistivity was caused by the difference of hygroscopicity, but this expectation was not accepted since the coverage of water for $ZrPLi_2$ was higher than that for $ZrPH_2$ as shown in Fig. 5. In Fig. 15, the humidity dependence of the activation energy on resistivity

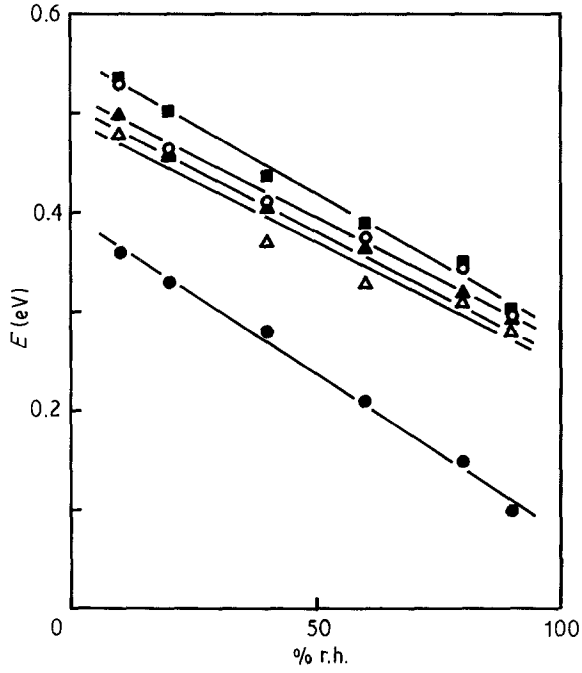

Figure 15 Humidity dependence of E. ● $ZrPH_2$, ○ $ZrPLi_2$, ▲ $ZRPNa_2$, △ $ZrPK_2$, ■ ZrPHNa.

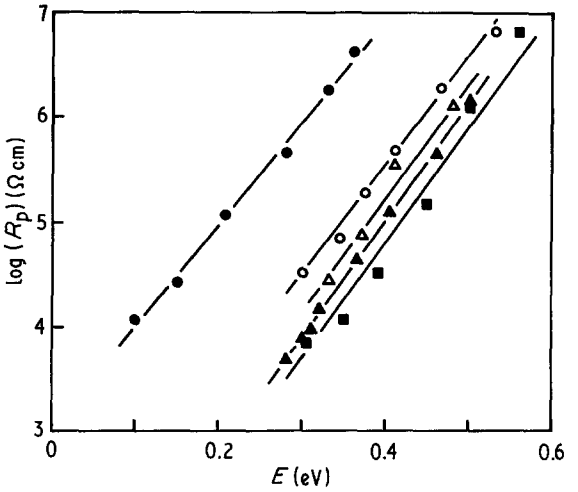

Figure 16 Relationship between R_p and E. ● $ZrPH_2$, ○ $ZrPLi_2$, ▲ $ZrPNa_2$, △ $ZrPK_2$, ■ ZrPHNa.

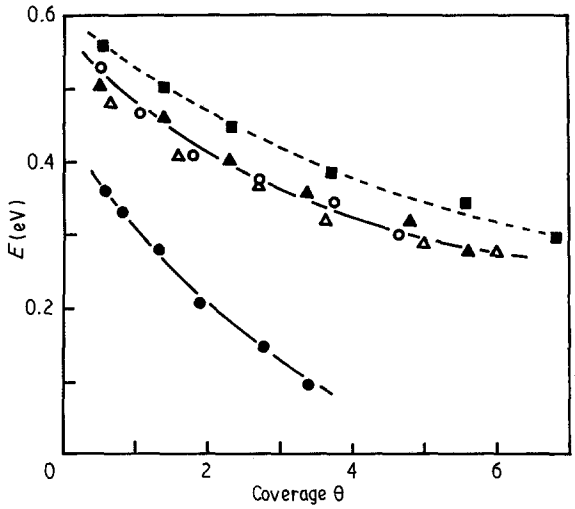

Figure 17 Activation energy dependence on the coverage of the physiosorbed water. ● $ZrPH_2$, ○ $ZrPLi_2$, ▲ $ZrPN_a$, △ $ZrPK_2$, ■ ZrPHNa.

was shown. The activation energy decreased monotonically with increasing humidity and increased by replacing the acidic protons with monovalent alkali cations. For each sample the value of R_p increased with an increase in the activation energy and the resistivity could be expressed by Equation 6 as shown in Fig. 16. The estimated value of R^* decreased by replacing the acidic protons with alkali cations (Table I). In Fig. 17 the activation energy dependence on the coverage of water was shown. The activation energy for the full and half ion exchanged was higher than that for CZP100 (H-form), while a distinct difference in the alkali species was not confirmed.

For alkali forms, the activation energy for $ZrPLi_2$, $ZrPNa_2$ and $ZrPK_2$ was determined to be 0.63 eV, 0.68 eV and 0.91 eV by Yamanaka [25] and 0.68 eV, 0.71 eV and 0.93 eV by Casciola and Fabiani [12], respectively. All of the reported values were obtained for temperatures above ca. 150° C. As shown in Fig. 5, the weight loss observed below 150° C and then the weight become constant for $ZrPNa_2$ and $ZrPK_2$. The distinction between the value obtained in this work and others may be caused by the difference in water contents. It seems that the alkali cation and the proton act as the charge carrier while the degree of contribution of the alkali cations and protons to the conduction cannot be determined. Preliminary effects of the monovalent cation species on the impedance–humidity relation for the zircon and the other oxide fired with phosphoric acid or its mono-alkali salt [6, 26] were examined and it was confirmed that the activation energy for conduction was only dependent on the coverage of water and hardly influenced by the monovalent cation species (hydrogen, sodium, potassium). For these samples, most of the phosphate is modified only on the particle surfaces and the conduction path was limited to the particle surfaces. These confirmed results showed that the main charge carriers were the protons produced by the dissociation of the physisorbed water. However, in this work, the activation energy increased by replacing the acidic protons with alkali cations. This discrepancy indicates that the alkali cation acts as a charge carrier and the conduction occurs not only on the particle surfaces but also in the crystals. This interpretation, i.e. the diversification of the conduction mechanism, convinced us of the increase in the θ value (Table II) caused by replacing the proton with alkali cations. As shown in Table I, the value of R^* decreased and the interlayer distance increased when the proton was replaced by the monovalent cations. It seems that the decrements of R^* are caused by the increase in the conductive path by the extent of the interlayer distance, since the surface area of the samples prepared from CZP100 is hardly dependent on the monovalent cation species and the distinction of particle size and/or surface area is removed as the origin of the difference of R^*. However, at the present time, it is difficult to discuss in more detail, since similar decrements have been observed in zircon-dihydrogen monoalkali phosphate systems [6].

References

1. T. NITTA, Z. TERADA and S. HAYAKAWA, *J. Amer. Ceram. Soc.* **63** (1980) 295.
2. Y. SHIMIZU, H. ARAI and T. SEIYAMA, *Denki Kagaku* **50** (1982) 831.
3. Y. SADAOKA and Y. SAKAI, *ibid.* **51** (1983) 879.
4. F. UCHIKAWA and K. SHIMAMOTO, *Amer. Ceram. Soc. Bull.* **64** (1985) 1137.
5. Y. SADAOKA and Y. SAKAI, *J. Mater. Sci.* **20** (1985) 3027.
6. *Idem., J. Mater. Sci. Lett.* **5** (1986) 656.
7. Y. SADAOKA, M. MATSUGUCHI, Y. SAKAI and S. MITSUI, in Proc. Int. Conf. Solid-State Sensors and Actuators, Tokyo, 1987, p. 673.
8. D. BIANCHI and M. CASCIOLA, *Solid State Ionics* **17** (1985) 7.
9. Y. SADAOKA, M. MATSUGUCHI, Y. SAKAI and S. MITSUI, *J. Mater. Sci.* **22** (1987) 2975.
10. G. ALBERTI and U. CONSTANTINO, *J. Chromatogr.* **102** (1974) 5.
11. A. DYER, D. LEIGH and F. T. OCON, *J. Inorg. Nucl. Chem.* **33** (1971) 3141.
12. M. CASCIOLA and D. FABIANI, *Solid State Ionics* **11** (1983) 31.
13. W. MEYER and H. NELDEL, *Z. Tech. Phys.* **12** (1937) 588.
14. R. DEWSBERRY, *J. Phys. D* **8** (1975) 1797.
15. B. ROSENBERG, B. BHOWMIK, H. C. HARDER and E. POSTOW, *J. Chem. Phys.* **49** (1968) 4108.
16. K. L. NARASIMHAN and B. M. ARORA, *Solid State*

Commun. **55** (1985) 615.
17. J. C. DYRE, *J. Phys. C* **19** (1986) 5655.
18. T. DOSDALE and R. J. BROOK, *Solid State Ionics* **8** (1983) 297.
19. H. SCHER and M. LAX, *Phys. Rev.* **B7** (1973) 4491.
20. U. CONSTANTINO, L. SZIRTES and J. KÖRNYEI. *J. Chromatogr.* **201** (1980) 167.
21. Y. SADAOKA and Y. SAKAI, *Hyomen Kagaku* **5** (1984) 220.
22. *Idem., J. Mater. Sci. Lett.* **5** (1986) 656.
23. G. ALBERTI, M. CASCIOLA, U. CONSTANTINO and M. LEONARDI, *Solid State Ionics* **14** (1984) 289.
24. E. K. ANDERSON, I. G. K. ANDERSON, C. K. MØLLER, K. E. SIMONSEN and E. SKOU, *ibid.* **7** (1982) 301.
25. S. YAMANAKA, *J. Inorg. Nucl. Chem.* **42** (1980) 717.
26. Y. SADAOKA, M. MATSUGUCHI, Y. SAKAI, H. AONO, S. NAKAYAMA and H. KUROSHIMA, *J. Mater. Sci.* **22** (1987) 3685.

Received 26 May
and accepted 22 October 1987